PHYSICAL REVIEW LETTERS **135,** 026201 (2025)

Editors' Suggestion

Quantum Stochastic Rectification in a Single Molecule

Jiang Yao,[1] Siyu Chen,[1] Wenlu Shi,[1] and W. Ho[1,2,*]
[1]*Department of Physics and Astronomy, University of California, Irvine, California 92697-4575, USA*
[2]*Department of Chemistry, University of California, Irvine, California 92697-2025, USA*

(Received 24 February 2025; accepted 14 June 2025; published 7 July 2025)

Quantum stochastic rectification arises from the dc response of a system subjected to both quantum noise and a small, periodic sinusoidal voltage modulation. In this Letter, we demonstrate quantum stochastic rectification by using inelastic electron tunneling spectroscopy with a scanning tunneling microscope to monitor the conformational switching of a single pyrrolidine molecule adsorbed on a Cu(001) surface. By applying quasistatic and nonequilibrium approximations, we elucidate the underlying dynamic response mechanisms. Additionally, we establish a quantitative relationship between the critical driving frequency in rectification measurements and the system's relaxation time, facilitating the measurement of rapid relaxation rates in single molecules.

DOI: 10.1103/dqfn-y77k

Quantum noise, a fundamental aspect of quantum mechanics, can induce stochastic switching in two-level systems. With the rapid advancement of quantum computing and communication technologies, the study of quantum noise has garnered increased attention [1–5]. One method to characterize quantum noise is by examining the interaction between a periodic force and stochastic systems driven by this noise. The most recognized phenomenon in such systems is quantum stochastic resonance, which predicts maximum synchronization efficiency at a specific periodic driving frequency [6–10]. Although the theory of quantum stochastic resonance was established in 1994 [6], experimental observations have only recently been reported [9,10]. Investigating synchronization efficiency remains challenging due to the limited detection speed of electronics, especially when quantum stochastic dynamics occur at the picosecond scale [11,12]. Consequently, measuring the dc response of quantum stochastic systems through quantum stochastic rectification has become an effective approach. However, previous studies often overlook the rectification term since it appears only as a second-order approximation [13–16]. To our knowledge, the only theoretical study providing an analytic expression for stochastic rectification is valid under specific conditions (see Supplemental Material [17] for proof) [20], and a comprehensive study of quantum stochastic rectification has yet to be undertaken.

We utilized a custom-built scanning tunneling microscope (STM) to measure the rectification spectra, $I_R(V)$, of an isolated single pyrrolidine molecule adsorbed on a Cu(001) surface at 10 K [Fig. 1(a)]. Figure S10B shows the topography of a single pyrrolidine molecule. The adsorbed pyrrolidine molecules exhibit stochastic conformational switching, driven by external quantum noise from inelastic electron tunneling, which introduces distinct nonlinearity in the $I(V)$ curve [21–24]. Rectification spectroscopy captures this nonlinearity [25–27], revealing different spectral line shapes at varying bias modulation frequencies. We demonstrate that these phenomena are linked to the dynamic response of the single molecule's conformational state probability. A quantitative understanding of the rectification spectroscopy results was achieved by comparing numerical and analytical solutions under different approximations. We further measured $I_R(V)$ as a function of bias modulation frequencies, $I_R(V, f)$, and developed an accurate analytical expression for stochastic rectification. Additionally, we established a quantitative relationship between the critical frequency of $I_R(V, f)$ and the relaxation time (T_1) of the bistable two-level system.

Previous studies have shown that $I_R(V)$ of a single molecule resembles its inelastic electron tunneling spectroscopy (IETS) because both spectroscopies measure the nonlinearity in the $I(V)$ curve, and their second-order approximations are equivalent to (d^2I/dV^2) [25–29]. The negative differential resistance (NDR) characteristic of a pyrrolidine molecule in a tunneling junction contributes to this $I(V)$ nonlinearity [21–23]. Both IETS [Fig. 1(b)] and $I_R(V)$ [Fig. 1(c)] capture the NDR near ±368 mV. Interestingly, the low-bias modulation frequency (low-f) $I_R(V)$ resembles the line shape of IETS, but it differs from the $I_R(V)$ obtained at high bias modulation frequency (high-f). To understand these differences, it is necessary to examine the origin of the NDR.

The pyrrolidine NDR features arise from its stochastic switching between two conformational states, high (H) and low (L) [Fig. 2(a)] [21–24]. We monitored this switching process by recording the pyrrolidine tunneling current trace

---

[*] Contact author: wilsonho@uci.edu

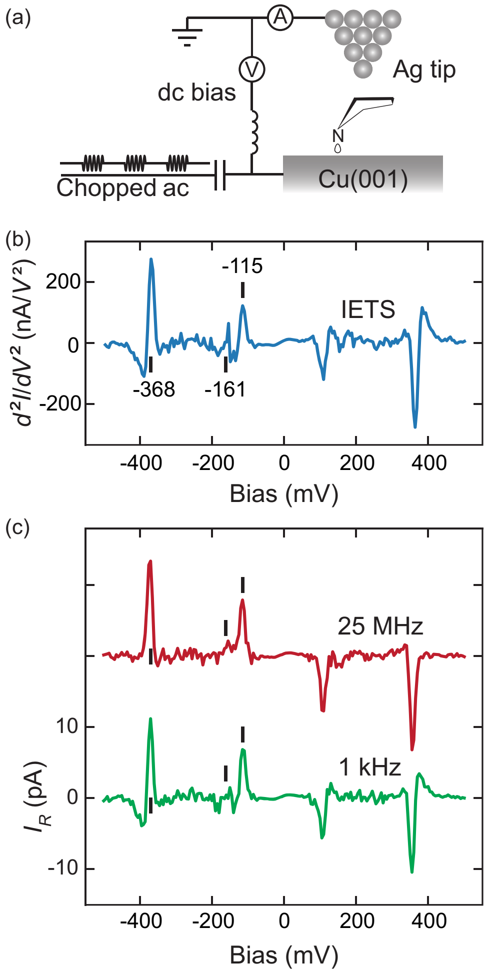

FIG. 1. Inelastic electron tunneling spectroscopy (IETS) and rectification spectroscopy of a single pyrrolidine molecule on Cu(001). (a) Schematic diagram of the rectification measurement setup. The high-frequency ac bias modulation was square-wave chopped at 320 Hz (chopping frequency) and applied to the Cu(001) substrate with a dc bias. The rectification current was extracted using a lock-in amplifier to measure the tunneling current oscillating at the chopping frequency. All rectification measurements were performed with 320 Hz chopping of the ac carrier oscillation, with an amplitude of 14.1 mV measured outside the vacuum system and applied to the bias. (b) IETS of pyrrolidine recorded using the conventional second harmonic lock-in technique [28], with a sinusoidal bias modulation of 320 Hz and an amplitude of 14.1 mV. (c) Rectification spectra of pyrrolidine at two carrier frequencies (1 kHz and 25 MHz). All pyrrolidine measurements presented in this Letter were conducted with a -500 mV/1 nA setpoint and an open feedback loop unless otherwise specified.

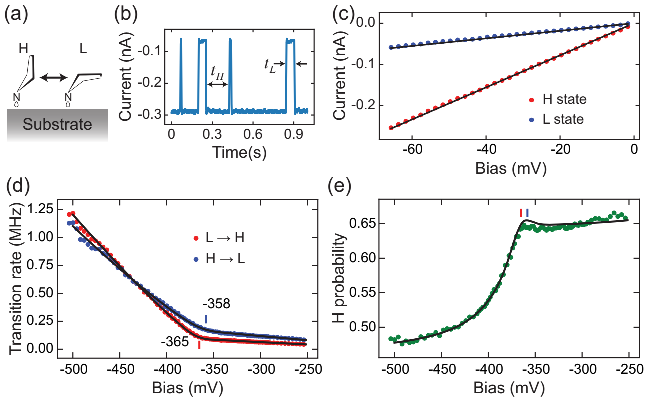

FIG. 2. Pyrrolidine switching dynamics. (a) Schematic diagram illustrating the switching between high (H) and low (L) conformational states of pyrrolidine. (b) Constant tip height current trace recorded over the center of a pyrrolidine molecule, measured at a -78 mV sample bias. The high and low current levels correspond to the H and L states, respectively. (c) State-resolved $I(V)$ obtained from the current traces. The slopes from the linear fits (solid lines) indicate conductance values of 3.90 nS for the H state and 0.92 nS for the L state. (d) Pyrrolidine transition rates as a function of bias. (e) H state probability as a function of bias. The solid black curves in (d) and (e) are fits based on the inelastic tunneling-assisted switching model (see Supplemental Material [17] for fitting details). The short vertical lines indicate the fitted vibrational energies for the C-H stretch in the H (358 meV) and L (365 meV) conformational states. Data in (d) and (e) were obtained using the pulse count method developed for measuring high transition rates (see Supplemental Material [17]).

with a constant tip height [Fig. 2(b)]. The high and low current levels correspond to the molecule in H and L states, respectively. The state-resolved $I(V)$ relation indicates constant conductance values for the H and L states, σ_H and σ_L [Fig. 2(c)]. Moreover, the conformational switching process can be facilitated by exciting C-H stretch vibrational modes through inelastic electron tunneling (IET) [21–23]. This effect causes a change in the transition rates $W_{H\to L(L\to H)}$, which are the inverses of the average residence times $t_{H(L)}$ of the corresponding states (see Supplemental Material [17]), as a function of bias at the C-H stretch excitation energies [Fig. 2(d)]. IET asymmetrically influences the conformational transitions, resulting in different kink positions and slope changes for $W_{H\to L(L\to H)}(V)$ as a function of bias [Fig. 2(d)]. This asymmetry modulates the H state occupation percentage [Fig. 2(e)] according to Eq. (1). The H state occupation is also the probability of finding the molecule in the H state long after any transition rate changes, denoted as $n_{H,\infty}$ (see Supplemental Material [17]).

$$H\,\text{occupation}\% = \frac{W_{L\to H}(V)}{W_{L\to H}(V) + W_{H\to L}(V)} = n_{H,\infty}(V). \tag{1}$$

The total tunneling current is the statistical average of the H and L state tunneling currents:

$$\begin{aligned} I(V) &= [n_{H,\infty}(V)\sigma_H + n_{L,\infty}(V)\sigma_L]V \\ &= [n_{H,\infty}(V)\Delta\sigma + \sigma_L]V. \end{aligned} \tag{2}$$

In Eq. (2), we use the normalization condition $n_{H,\infty}(V) + n_{L,\infty}(V) = 1$, and $\Delta\sigma = \sigma_H - \sigma_L$. As electron energy increases, the rapid decrease of $n_{H,\infty}$ around -368 mV [Fig. 2(e)] causes a decrease in the total tunneling current, leading to NDR.

The NDR features in the low-f $I_R(V)$ appear as a peak at -368 mV with an overshoot at lower bias [Fig. 3(a)]. In contrast, high-f $I_R(V)$ shows a stronger signal on the low-bias side of the NDR feature, resulting in a wider peak [Fig. 3(a)]. To reproduce the $I_R(V)$ line shapes, we introduce a set of differential equations [Eq. (3)] to characterize the time evolution of state probability, $n_{H(L)}(V,t)$, under a sinusoidal bias modulation, $V_m \cos(2\pi f t)$.

$$\frac{\partial}{\partial t}\begin{pmatrix} n_H(V,t) \\ n_L(V,t) \end{pmatrix} = \begin{pmatrix} -W_{H\to L}(V + V_m\cos(2\pi f t)) & W_{L\to H}(V + V_m\cos(2\pi f t)) \\ -W_{L\to H}(V + V_m\cos(2\pi f t)) & W_{H\to L}(V + V_m\cos(2\pi f t)) \end{pmatrix}\begin{pmatrix} n_H(V,t) \\ n_L(V,t) \end{pmatrix}. \tag{3}$$

According to Eq. (2), the tunneling current with bias modulation, $I(V,t)$:

$$I(V,t) = [n_H(V,t)\Delta\sigma + \sigma_L][V + V_m\cos(2\pi f t)]. \tag{4}$$

The dc component of the tunneling current, $I_R(V)$, is measured in the presence of ac bias modulation [26]:

$$I_R(V) = f\int_0^{1/f} I(V,t)dt - I(V). \tag{5}$$

By combining Eqs. (4) and (5), and the numerical solution to Eq. (3), we calculated the high- and low-frequency $I_R(V)$ [Fig. 3(b)], which matched the experimental results [Fig. 3(a)].

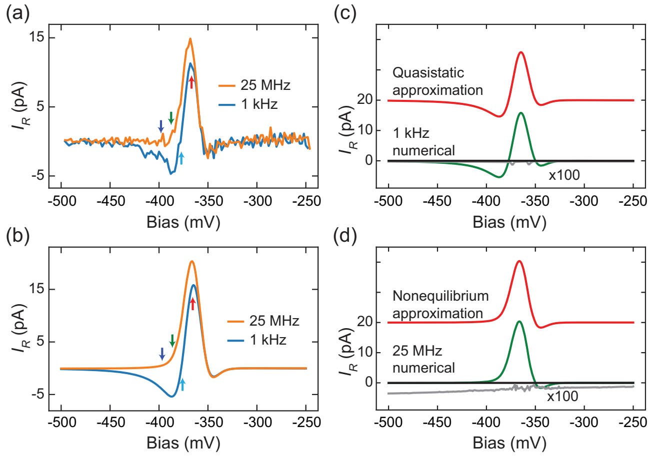

FIG. 3. Pyrrolidine rectification spectra at low and high bias modulation frequency limit. (a) Measured and (b) numerically calculated rectification spectra of pyrrolidine at two different bias modulation frequencies (1 kHz and 25 MHz). (c) Comparison between the analytical solution under the quasistatic approximation [see Supplemental Material [17], Eq. (S14)] and the 1 kHz numerical solution. (d) Comparison between the analytical solution under the nonequilibrium approximation [see Supplemental Material [17], Eq. (S16)] and the 25 MHz numerical solution. The black curves in (c) and (d) represent the difference between the green and red spectra in the respective figures. The gray curves are the amplified versions of the black curves (amplified by 100 times). All red curves have been shifted vertically for clarity.

To intuitively understand the frequency-dependent spectral line shape change of $I_R(V)$, we further examine the analytical solution to Eq. (3) without bias modulation [$(V_m = 0)$:

$$\begin{aligned} n_H(V,t) = {} & (n_H(V,t_0) - n_{H,\infty})e^{-(W_{L\to H}(V)+W_{H\to L}(V))(t-t_0)} \\ & + n_{H,\infty}(V). \end{aligned} \tag{6}$$

Equation (6) indicates that, upon any instant transition rate variation, the H state probability exponentially approaches the new equilibrium value, $n_{H,\infty}(V)$, with a decay rate of $W_{L\to H}(V) + W_{H\to L}(V)$. When the bias modulation frequency is sufficiently low $f \ll W_{L\to H}(V) + W_{H\to L}(V)$], $n_H(V,t)$ decays much faster than the bias variation. Thus, at any moment during bias modulation, n_H can reach its equilibrium value, $n_{H,\infty}$ (quasistatic approximation), and $n_H(V,t)$ takes the form of $n_{H,\infty}[V + V_m\cos(2\pi f t)]$. This approximation characterizes the low-f behavior of $I_R(V)$ [Fig. 3(c)] and explains its similarity to IETS: both modulate the bias slowly and reflect the characteristics of the equilibrium tunneling current. Their second-order approximations (both equal to $(V_m^2/4)(d^2I/dV^2)$) are independent of the bias modulation frequencies [25,26].

When the bias modulation frequency is sufficiently high [$f \gg W_{L\to H}(V) + W_{H\to L}(V)$], according to the exponential time response described in Eq. (6), n_H does not have enough time to vary significantly within each bias modulation cycle. Consequently, n_H only responds to the dc components of $W_{L\to H(H\to L)}[V + V_m\cos(2\pi f t)]$. To further analyze this, we expand the transition rates around the dc bias V using a Fourier series:

$$\begin{aligned} & W_{L\to H(H\to L)}(V + V_m\cos(2\pi f t)) \\ & \quad = W_{L\to H(H\to L)}(V) + W_{L\to H(H\to L),R}(V) \\ & \qquad + W_{L\to H(H\to L),f}(V)\cos(2\pi f t) \\ & \qquad + W_{L\to H(H\to L),2f}(V)\cos(4\pi f t) \\ & \qquad + \ldots(\text{higher harmonic terms}). \end{aligned} \tag{7}$$

The second dc term in Eq. (7), which is the rectification term of $W_{L\to H(H\to L)}$, arises from the nonlinearity of $W_{L\to H(H\to L)}(V)$. This term influences n_H and leads to the observed features in high-f $I_R(V)$ (nonequilibrium approximation). By retaining only the dc terms in Eq. (7) for the I_R calculation, we numerically reproduce the features of the high-f $I_R(V)$ [Fig. 3(d)].

To study the transition in the line shape of $I_R(V)$, we measured $I_R(f)$ at four different biases, each showing a step transition [Fig. 4(a)]. The line shape of $I_R(f)$ can be described by a Lorentzian function that peaks at 0 Hz with a critical frequency, f_0, which corresponds to the midpoint of the step transition. The numerically calculated $I_R(f)$, based on Eq. (3), exhibits the same line shape [Fig. 4(b)]. Thus, we constructed a Lorentzian expression to characterize $I_R(V,f)$:

$$I_R(V,f)=I_R(V,f=\infty)+\frac{I_R(V,f=0)-I_R(V,f=\infty)}{1+(f/f_0)}. \tag{8}$$

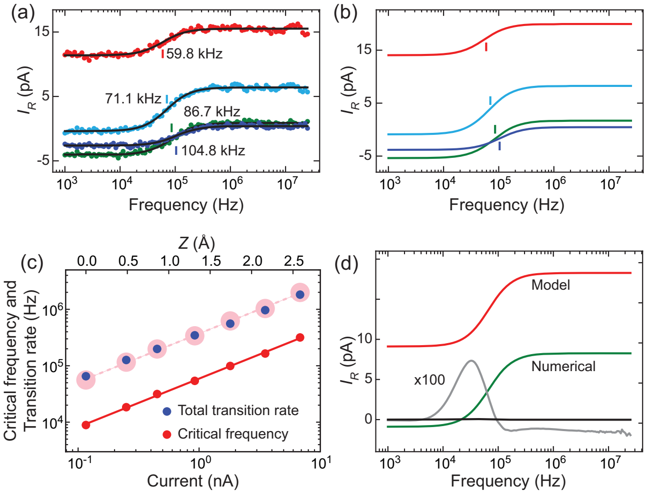

FIG. 4. Filtering model of pyrrolidine rectification. (a) Measured and (b) numerically calculated I_R of pyrrolidine as a function of bias modulation frequency at different biases. The biases (−398, −388, −378, and −368 mV) are color coded as red, cyan, green, and blue, respectively. The solid black curves in (a) represent Lorentzian fits (see Supplemental Material [17] for fitting details). The critical frequency for each bias is marked with a short vertical line. (c) Critical frequency (red dots) and corresponding total transition rate (blue dots) from the I_R frequency scan at different tunneling gaps (see Supplemental Material [17], Fig. S9 for raw data). The critical frequencies are derived from the Lorentzian fit in Fig. S9. The red line represents a power law fit (Critical frequency $= 80.4I^{0.86}$). The pink solid circles and pink dashed line indicate the critical frequencies and their fitting results multiplied by 2π. (d) I_R as a function of bias modulation frequency, calculated based on Eq. (8) (model) and the numerical solution to Eq. (3) (numerical). The bias chosen for the calculation is −378 mV. The black curve in (d) represents the difference between the green and red spectra. The gray curve shows the black curve amplified by 100 times. The red spectrum has been shifted vertically for clarity.

The low- and high-frequency limits of $I_R(V)$, $I_R(V,f=0)$ and $I_R(V,f=\infty)$, correspond to the results obtained from the quasistatic and nonequilibrium approximations.

In Eq. (8), only the physical meaning of f_0 remains undefined, so we reexamine the exponential time response in Eq. (6). According to the Fourier transform, an exponential decay in the time domain results in a Lorentzian response in the frequency domain, with a characteristic frequency equal to the exponential decay rate divided by 2π. Similar to an RC circuit, a step voltage change causes an exponential current decay in time, and the current response to an ac voltage is Lorentzian in the frequency domain with a critical frequency of $1/(2\pi RC)$. Therefore, we predict the critical frequency of $I_R(f)$ to be $[W_{L\to H}(V)+W_{H\to L}(V)]/2\pi$.

To verify this relationship, we varied the pyrrolidine transition rates across a wide range by adjusting the tunneling gap and found that the total switching rate, $W_{L\to H}+W_{H\to L}$, closely matched $2\pi f_0$ [Fig. 4(c)]. The power-law relationship between f_0 and tunneling current observed in Fig. 4(c) originates from IET-induced single molecule switching [30–32]. Figure 4(d) shows the high accuracy between the simplified Lorentzian expression for $I_R(V,f)$ [Eq. (8)] and its exact numerical calculation (with an error of less than 1%), further validating our analysis. This method for deriving $I_R(V,f)$ can also be applied to construct the rectification of n_H as a function of bias modulation frequency and bias (see Supplemental Material [17]).

Equation (3) has been widely used to describe the relaxation process of bistable systems [33–35]. The inverse of $W_{L\to H}+W_{H\to L}$ characterizes the system relaxation time (T_1). Using this frequency-dependent I_R measurement, we can further determine T_1 with the simple relation $T_1=(1/2\pi f_0)$. It is worthwhile to compare this technique with the conventional T_1 measurement method—electric pulse pump-probe technique [36–38]. In practice, frequency-dependent phase lag and signal loss in electrical transmission can distort pulse shapes and limit the use of short pulses, thereby restricting the temporal resolution of the pump-probe technique.

In contrast, the $I_R(f)$ measurement uses a sinusoidal signal, which is less sensitive to phase lag. The frequency-dependent signal loss can also be calibrated with a compensation method (see Supplemental Material [17]). Therefore, compared to the electric pump-probe technique, the frequency-dependent I_R method can measure shorter T_1 values using the same electrical setup. Additionally, unlike electrical voltage pulses, sinusoidal bias modulation is a pure ac signal that can be introduced into the STM junction via antenna coupling. Photoconductive antennas can emit sinusoidal electrical signals up to a few THz [39–41]. Previous studies have shown the successful coupling of THz radiation into an STM junction (THz-STM) [42,43]. By combining continuous-wave (cw) THz-STM with this rectification technique, we expect subpicosecond relaxation dynamics to be measurable at the atomic scale. A recent stochastic resonance study on a single iron atom also observed changes in spin state probability as a function of bias modulation frequency, claiming it as the sole contributor to changes in dc tunneling current [10]. However, our theoretical analysis indicates that, at low frequencies, the first harmonic state probability oscillation also contributes to changes in the dc tunneling current (see Supplemental Material [17]). Their claim may be a rough approximation under specific circumstances (e.g., $V \gg V_m$). Furthermore, they did not establish the relationship between f_0 and relaxation time.

Previous theories of quantum stochastic resonance have relied on the assumption that the coherence timescale is much shorter than the timescale associated with quantum noise-induced switching. Because of the limitations in detection techniques, dynamics occurring on timescales comparable to coherence have been difficult to resolve in real time—currently the dominant method for probing switching behavior. As a result, existing theories have remained unchallenged. In this Letter, we establish the foundation for quantum stochastic rectification, which enables the detection of extremely fast switching dynamics, potentially down to the subpicosecond regime—on par with the coherence timescales of many systems. The physics within this overlapping timescale region has not been previously explored, and our results pave the way for investigating the interplay between coherence and quantum stochastic resonance.

In summary, we examined the frequency-dependent rectification of a single pyrrolidine molecule. This frequency dependence arises from the dynamic response of pyrrolidine conformational switching, driven by inelastic tunneling electrons. The low- and high-frequency $I_R(V)$ results align with the quasistatic and nonequilibrium approximations. We also developed an analytic expression to describe the step transition of the stochastic rectification current in the frequency domain. The critical frequency of $I_R(f)$ characterizes the bistable system's relaxation time through the relation $T_1 = (1/2\pi f_0)$. This novel technique enables the measurement of faster relaxation (switching) processes in bistable systems.

Acknowledgments—This work was supported by the Office of Basic Energy Sciences of the U.S. Department of Energy Award No. DE-SC0024037. We have additionally benefitted from discussions and suggestions by Yunpeng Xia, Likun Wang, and Dan Bai.

Data availability—The data that support the findings of this article are not publicly available. The data are available from the authors upon reasonable request.

[1] C. H. Henry and R. F. Kazarinov, Rev. Mod. Phys. **68**, 801 (1996).

[2] R. Alicki, M. Horodecki, P. Horodecki, and R. Horodecki, Phys. Rev. A **65**, 062101 (2002).

[3] E. Knill, Nature (London) **434**, 39 (2005).

[4] R. Harper, S. T. Flammia, and J. J. Wallman, Nat. Phys. **16**, 1184 (2020).

[5] Y. Du, M.-H. Hsieh, T. Liu, D. Tao, and N. Liu, Phys. Rev. Res. **3**, 023153 (2021).

[6] R. Löfstedt and S. N. Coppersmith, Phys. Rev. Lett. **72**, 1947 (1994).

[7] M. Grifoni and P. Hänggi, Phys. Rev. Lett. **76**, 1611 (1996).

[8] I. Goychuk and P. Hänggi, Phys. Rev. E **59**, 5137 (1999).

[9] T. Wagner, P. Talkner, J. C. Bayer, E. P. Rugeramigabo, P. Hänggi, and R. J. Haug, Nat. Phys. **15**, 330 (2019).

[10] M. Hänze, G. McMurtrie, S. Baumann, L. Malavolti, S. N. Coppersmith, and S. Loth, Sci. Adv. **7**, eabg2616 (2022).

[11] Z. Y. Xu and C. L. Tang, Appl. Phys. Lett. **44**, 692 (1984).

[12] Y. Nishikawa, A. Tackeuchi, S. Nakamura, S. Muto, and N. Yokoyama, Appl. Phys. Lett. **66**, 839 (1995).

[13] B. McNamara and K. Wiesenfeld, Phys. Rev. A **39**, 4854 (1989).

[14] L. Gammaitoni, P. Hänggi, P. Jung, and F. Marchesoni, Rev. Mod. Phys. **70**, 223 (1998).

[15] J. Li, Phys. Rev. E **66**, 031104 (2002).

[16] Y.-F. Guo, Y.-J. Shen, and J.-G. Tan, Mod. Phys. Lett. B **29**, 1550034 (2015).

[17] See Supplemental Material at http://link.aps.org/supplemental/10.1103/dqfn-y77k, which includes Refs. [18,19], for additional information about materials and method; frequency scan with constant amplitude bias modulation in the tunneling junction; transition rates and Poisson distribution; pulse count method to measure fast switching dynamics; inelastic electron tunneling assisted conformational transitions; protocol for numerical calculation of rectification current; stochastic rectification current; state probability as a function of frequency; stochastic rectification of state probability; single-molecule topography; rectification spectra positive and negative bias symmetry; and experiment, simulation, and model.

[18] J. Lambe and R. C. Jaklevic, Phys. Rev. **165**, 821 (1968).

[19] J. Klein, A. Léger, M. Belin, D. Défourneau, and M. J. L. Sangster, Phys. Rev. B **7**, 2336 (1973).

[20] R. Löfstedt and S. N. Coppersmith, Phys. Rev. E **49**, 4821 (1994).

[21] J. Gaudioso, L. J. Lauhon, and W. Ho, Phys. Rev. Lett. **85**, 1918 (2000).

[22] J. Gaudioso and W. Ho, Angew. Chem. **113**, 4204 (2001).

[23] J. Gaudioso and W. Ho, J. Am. Chem. Soc. **123**, 10095 (2001).

[24] S. Li, S. Chen, J. Li, R. Wu, and W. Ho, Phys. Rev. Lett. **119**, 176002 (2017).

[25] J. Lee, X. Tu, and W. Ho, Nano Lett. **5**, 2613 (2005).

[26] X. W. Tu, J. H. Lee, and W. Ho, J. Chem. Phys. **124**, 21105 (2006).

[27] D. R. Ward, F. Hüser, F. Pauly, J. C. Cuevas, and D. Natelson, Nat. Nanotechnol. **5**, 732 (2010).

[28] B. C. Stipe, M. A. Rezaei, and W. Ho, Science **280**, 1732 (1998).

[29] W. Ho, J. Chem. Phys. **117**, 11033 (2002).

[30] B. C. Stipe, M. A. Rezaei, and W. Ho, Science **279**, 1907 (1998).

[31] K. Motobayashi, Y. Kim, H. Ueba, and M. Kawai, Phys. Rev. Lett. **105**, 076101 (2010).
[32] J. Oh, H. Lim, R. Arafune, J. Jung, M. Kawai, and Y. Kim, Phys. Rev. Lett. **116**, 056101 (2016).
[33] R. C. Hilborn, Am. J. Phys. **50**, 982 (1982).
[34] P. T. Landsberg and A. G. Guy, Phys. Rev. B **28**, 1187 (1983).
[35] J. Mompart and R. Corbalán, Phys. Rev. A **63**, 063810 (2001).
[36] S. Loth, M. Etzkorn, C. P. Lutz, D. M. Eigler, and A. J. Heinrich, Science **329**, 1628 (2010).
[37] W. Paul, K. Yang, S. Baumann, N. Romming, T. Choi, C. P. Lutz, and A. J. Heinrich, Nat. Phys. **13**, 403 (2017).
[38] W. M. J. van Weerdenburg, M. Steinbrecher, N. P. E. van Mullekom, J. W. Gerritsen, H. von Allwörden, F. D. Natterer, and A. A. Khajetoorians, Rev. Sci. Instrum. **92**, 33906 (2021).
[39] R. Mendis, C. Sydlo, J. Sigmund, M. Feiginov, P. Meissner, and H. L. Hartnagel, Solid State Electron. **48**, 2041 (2004).
[40] R. Mendis, C. Sydlo, J. Sigmund, M. Feiginov, P. Meissner, and H. L. Hartnagel, IEEE Antennas Wireless Propag. Lett. **4**, 85 (2005).
[41] H. Tanoto, J. H. Teng, Q. Y. Wu, M. Sun, Z. N. Chen, S. A. Maier, B. Wang, C. C. Chum, G. Y. Si, A. J. Danner, and S. J. Chua, Sci. Rep. **3**, 2824 (2013).
[42] T. L. Cocker, D. Peller, P. Yu, J. Repp, and R. Huber, Nature (London) **539**, 263 (2016).
[43] W. Likun, X. Yunpeng, and W. Ho, Science **376**, 401 (2022).